Structural properties of a-SiO$_x$:H films studied by an improved infrared-transmission analysis method*

Wang Shuo(王 烁), Zhang Xiao-Dan(张晓丹), Xiong Shao-Zhen(熊绍珍), and Zhao Ying(赵 颖)†

Institute of Photo-electronic Thin Film Device and Technique, Nankai University, Tianjin 300071, *China*

(Received 5 February 2014; revised manuscript received 18 April 2014; published online 16 July 2014)

An improved method of fitting point-by-point is proposed to determine the absorption coefficient from infrared (IR) transmittance. With no necessity of empirical correction factors, the absorption coefficient can be accurately determined for the films with thin thicknesses. Based on this method, the structural properties of the hydrogenated amorphous silicon oxide materials (a-SiO$_x$:H) are investigated. The oxygen-concentration-dependent variation of the Si–O–Si and the Si–H related modes in a-SiO$_x$:H materials is discussed in detail.

Keywords: amorphous silicon oxide film, thin thickness, infrared transmission, structural properties

PACS: 88.40.H–, 78.30.–j, 78.20.Bh **DOI:** 10.1088/1674-1056/23/9/098801

1. Introduction

The hydrogenated amorphous silicon oxide (a-SiO$_x$:H) material is one of the most promising candidates to be used as the wide-gap absorber in the top cell to further improve the efficiency of silicon-based thin film tandem solar cells.[1,2] Infrared transmission has been used as an effective tool to analyze the structural properties and the bonding configurations of a-SiO$_x$:H,[3] as well as other silicon alloys.[4,5] In the early stage, the transmittance $T(\omega)$ was commonly converted to the absorption $\alpha(\omega)$ by the BCC and the CL methods proposed by Brodsky, Cardona, and Cuomo (BCC)[6] and by Connell and Lewis (CL),[7] assuming incoherent multiple reflections in the film and the substrate. These methods remain suitable under certain conditions. However, when the refractive index differs distinctly from that of the c-Si substrate because of the incorporation of O as well as other alloy elements such as C and Ge, the transmittance usually shows broad and shallow interference fringes in the baseline.[8–13] This will cause notable conversion errors when applying the BCC or CL method, especially when the thickness of the film is below a critical value.[14]

Maley proposed a semi-coherent model to suppress the interference fringes of the baseline of the spectrum.[14,15] Because of the lack of an analytical solution, the author converted $T(\omega)$ to $\alpha(\omega)$ by fitting the transmittance with Gaussian-like absorption peaks in a-Si:H. However, it is difficult to do it in this way when it comes to a-SiO$_x$:H materials, in which the infrared (IR) absorption peaks are much more complicated than those in a-Si:H. Thus, a method widely used is to fit the baseline by the Maley method and then convert $T(\omega)$ to $\alpha(\omega)$ by the BCC method[13,16] (which we call Maley–BCC or M–BCC method here). Although one can obtain $\alpha(\omega)$ with a flat baseline by using this method, it does not make sense theoretically, and it is necessary to reduce the errors by using films with large thicknesses (usually thicker than 1 μm). Maley also proposed a correction factor for films thinner than 1 μm, but it is effective only for a-Si films in theory.[14]

In this paper, we present a fast method for fitting the spectrum, point-by-point, to convert $T(\omega)$ to $\alpha(\omega)$ accurately based on the Maley model. With no necessity of correction factors, it is effective even when the film is very thin. Based on this method, the structural properties of a-SiO$_x$:H films with different oxygen concentrations are investigated in detail.

2. Experimental details

A series of a-SiO$_x$:H thin films with different oxygen concentrations were deposited on single-crystal Si substrates by very high frequency plasma enhanced chemical vapor deposition (VHF-PECVD) with SiH_4, H_2, and CO_2 as the reactive gases at the heater temperature of 195 °C. The oxygen concentration was modulated by varying the gas flow ratio $R_c = [CO_2]/[SiH_4]$ from 0 to 1.4. The deposition pressure and the VHF power were fixed at 0.5 Torr and 10 W, respectively. The IR transmittance was measured by a Fourier-transform spectrometer (FTS-6000 by Bio-Rad Inc., USA) from the layer stack under normal light incidence, as schematically illustrated in Fig. 1. The thicknesses of all the films, measured by a surface profiler, were around 300 nm.

*Project supported by the National Basic Research Program of China (Grant Nos. 2011CBA00705, 2011CBA00706, and 2011CBA00707), the National Natural Science Foundation of China (Grant No. 60976051), and the Program for New Century Excellent Talents in University of China (Grant No. NCET-08-0295).

†Corresponding author. E-mail: zhaoygds@nankai.edu.cn

© 2014 Chinese Physical Society and IOP Publishing Ltd

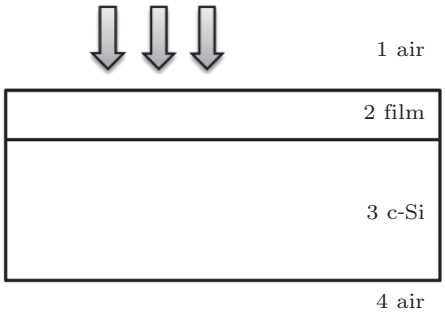


Fig. 1. Schematic diagram of layer stack in FTIR measurement.

3. Results

The transmittances of the layer stacks with different a-SiO_x:H films are shown in Fig. 2. Here the absorption in the c-Si substrate is taken into account by dividing the transmittance by that of the bare substrate, and then multiplying the non-absorbing transmittance of the c-Si substrate, 0.54. Consistent with the previous results,[17–20] the baselines of the spectra show stronger interference fringes with increasing gas flow ratio R_c.

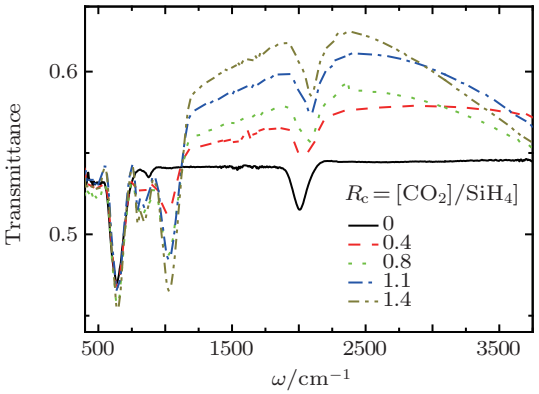


Fig. 2. Measured IR transmittances of the layer stacks with a-SiO_x:H films with different R_c.

3.1. Improved fitting of the baseline

First, the interference fringes in the spectra are eliminated by the semi-coherent model proposed by Maley.[14] The equation for the baseline can be obtained when the extinction coefficient of the a-SiO_x:H film (k_{film}) is set to be zero. By fitting the non-absorbing part of the transmittance spectrum with this equation, the effective refractive index and the thickness of the film, n_{film} and d_{film}, can be obtained. However, because of the refractive index dispersion of c-Si and the possible experimental error in the measurement, the results usually do not fit well enough with only these two parameters. There are big discrepancies between the measured and the fitted spectra, especially in the range of low wavenumbers, as shown in Fig. 3. So a third parameter, the effective refractive index of the c-Si substrate, n_{c-Si}, is introduced into the fitting, instead of being fixed at 3.42 as in the Maley method. By incorporating the third fitting parameter, the fitting quality is greatly improved, as shown in Fig. 3. The effective refractive index n_{c-Si} does not deviate much, but fluctuates around the value of 3.42 for different samples, as shown in the illustrated graph in Fig. 3. It can be treated as an indicator to evaluate the credibility of the fitting results.

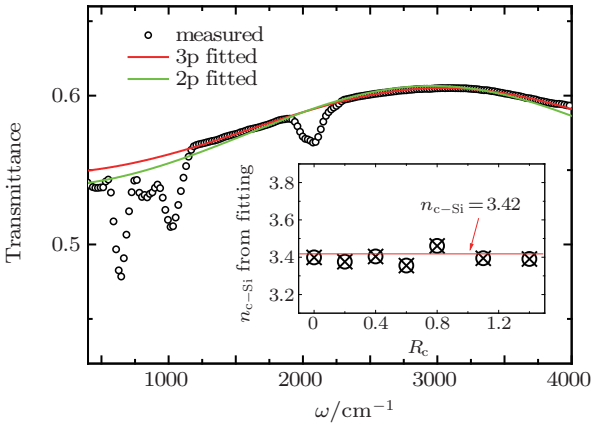


Fig. 3. Comparison between the baselines obtained by 2-parameter (2p) fitting and 3-parameter (3p) fitting. The inset shows the deviation of the effective refractive index of substrate for different samples.

3.2. Improved conversion from $T(\omega)$ to $\alpha(\omega)$

Secondly, we propose a method for fitting the transmittance at each wavenumber point-by-point (F-PbyP) to convert $T(\omega)$ to $\alpha(\omega)$. A flow chart of the procedure is shown in Fig. 4. In order to obtain the fitting rapidly and avoid the problem of multiple solutions, the fitting starts with zero as the initial value of k_{film} at the wavenumber of 4000 cm^{-1}, where no

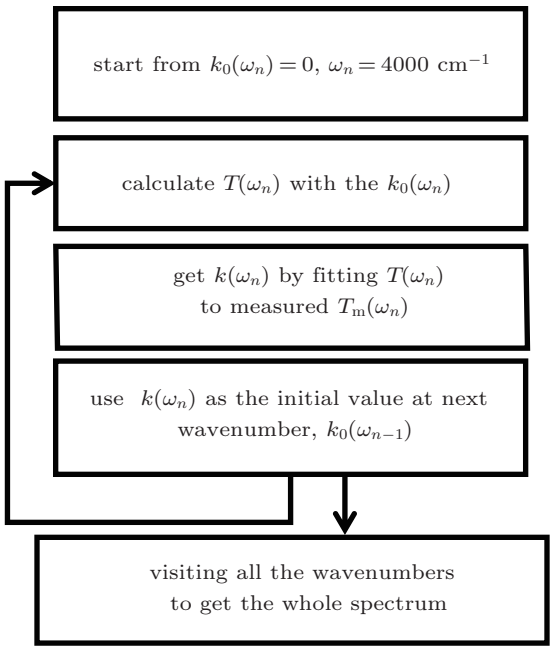


Fig. 4. Flow chart of the fitting point-by-point method to convert $T(\omega)$ to $\alpha(\omega)$, where ω is the wavenumber, k is the extinction coefficient of the a-SiO_x:H film, and T_m is the measured transmittance.

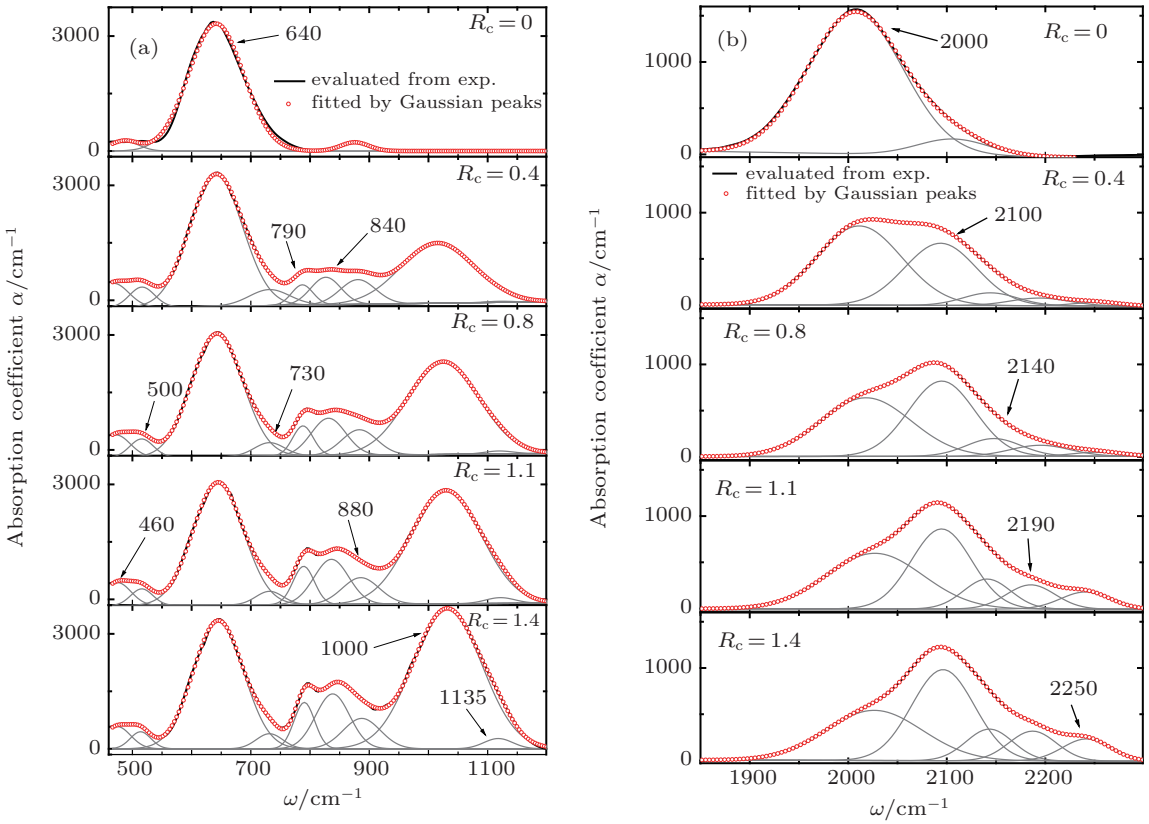


Fig. 5. Absorption coefficient spectra of a-SiOx:H films with different R_c evaluated by the F-PbyP method in the regions of (a) 460–1200 cm^{-1} and (b) 1850–2300 cm^{-1}. Each spectrum has been deconvoluted into probable satellite components by Gaussian peaks. The rough positions of the components are labeled with arrows.

absorption exists in the spectrum. The result of k_{film} of the previous wavenumber is used as the initial value for the fitting at the next lower wavenumber. By visiting all the wavenumbers in the spectrum, the whole spectrum of $k_{\text{film}}(\omega)$ can be obtained, as well as $\alpha_{\text{film}}(\omega)$ by $\alpha = 4\pi k/\lambda$. The procedure can be implemented easily by mathematical tools such as MATLAB. The absorption spectra with different R_c values, evaluated by the F-PbyP method, are shown by the black solid lines in Figs. 5(a) and 5(b).

4. Discussion

4.1. Error analysis

The effectiveness of the F-PbyP method will be discussed in this section. A set of parameters, $n_{\text{film}} = 3.1$, $n_{\text{c-Si}} = 3.42$, and $d_{\text{film}} = 300$ nm, the typical values for this series of a-SiO$_x$:H layers, is assumed. The dependence of k_{film} on ω is arbitrarily assumed to be composed of three Gaussian peaks at 1000 cm^{-1}, 2000 cm^{-1}, and 3000 cm^{-1}, respectively, and treated as the "real" $k(\omega)$ as shown in Fig. 6. The transmittance $T(\omega)$ of this film is calculated by the Maley model. Then $T(\omega)$ is converted to $k(\omega)$ by the BCC method, the M–BCC method, and the F-PbyP method respectively, as also shown in Fig. 6. The $k(\omega)$ obtained by the F-PbyP method agrees with the real value very well. However, the $k(\omega)$ obtained by the BCC method shows obvious coherent fringes and even has negative values in some regions.

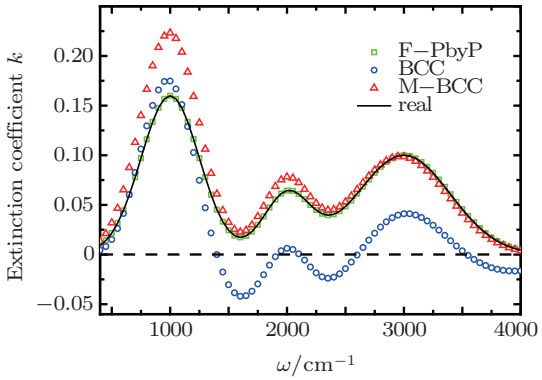


Fig. 6. Extinction coefficient evaluated from the transmittance spectrum by different methods. The transmittance spectrum is calculated by the semi-coherent model with assumed n_{film}, $n_{\text{c-Si}}$, d_{film}, and extinction coefficient of the film, k_{film}. The black solid line presents the assumed real k_{film}.

No coherent fringes are observed in the $k(\omega)$ obtained by the M-BCC method. However, it has relatively big errors in the low wavenumber region in this case. To further clarify the dependence of the errors on the film parameters of the M–BCC method, the relative error $E_r = (k_{\text{M-BCC}} - k_{\text{real}})/k_{\text{real}}$ is calculated by varying the refractive index and the thickness of the film. The k_{real} is the assumed real extinction coefficient and $k_{\text{M-BCC}}$ is the extinction coefficient evaluated by the M–BCC

method. As shown in Fig. 7(a), when the thickness of the film is fixed at 300 nm, the $k(\omega)$ obtained by the M–BCC method shows positive errors for most wavenumbers. The error can even be as big as +70% at around 640 cm^{-1} when the refractive index of the film equals 4 (possible for a-SiGe:H films). This will cause big errors when the hydrogen concentration is estimated from the Si–H rocking mode at this wavenumber. Figure 7(b) shows the dependence of the relative error on the thickness of the film when the reflective index is fixed at 3.1. When the film is as thin as 300 nm, there are errors up to +20% in the region of 500–2400 cm^{-1}, where most of the absorption peaks in silicon-based films exist. The error decreases with increasing film thickness and can be constrained within $\pm$10% when the film is thicker than 900 nm. However the fabrication of this kind of thick layer is quite time-consuming for the layers with low deposition rates. In contrast, none of these errors exist when applying the F-PbyP method.

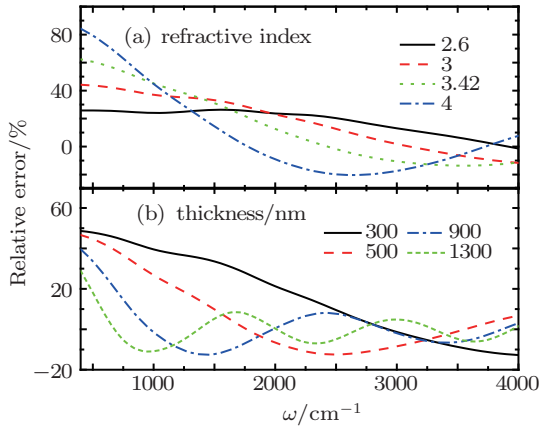


Fig. 7. Relative error between the real values and those from the M-BCC method for the films with (a) different refractive indexes and (b) different thicknesses.

4.2. FTIR analysis of a-SiO$_x$:H films

By means of the accurate F-PbyP method, the structural properties of the a-SiO$_x$:H films with different CO_2 to SiH_4 ratios are investigated. Two IR absorption bands in the regions of 460–1200 cm^{-1} and 1850–2300 cm^{-1} are deconvoluted into several possible satellite components by Gaussian fitting and shown in Figs. 5(a) and 5(b), respectively. An overview of the possible components used in the deconvolution is listed in Table 1. Most of them are confirmed by both the theoretical calculation and the experimental results of the previous studies. However, the origin of the peak at around 730 cm^{-1} is not so clear. It may come from the carbon-related stretching mode suggested by Babel *et al.*[21] or the lower bending mode of H–Si(SiO_2) calculated on the basis of a random-bonding model by He *et al.*[13] However neither of them can be proved in our studies. Further work on this peak in detail is necessary in the future.

Table 1. Possible assignments of vibrational modes in a-SiO$_x$:H films.

Peak position/cm^{-1}	Bonds	Vibrational mode and configuration
460[22]	Si–Si	stretching
500[23]	Si–O–Si	rocking
630–640[24]	Si–H	bending or rocking in SiH, SiH_2, $(SiH_2)_n$ or SiH_3
710–730	?	(not confirmed)
780–790[3,25]	Si–O–Si	bending
840–850[3,25]	Si–H	wagging in $(SiH_2)_n$ or bending in H–Si(O_2Si)
880–890[3,25]	Si–H	scissor in SiH_2or $(SiH_2)_n$ or bending in H–Si(O_3)
940–1050[3,21,25]	Si–O–Si	stretching in (Si–O–Si)-Si (single oxygen)
1135–1150[21,26,27]	Si–O–Si	stretching in O–Si(O_3) (oxygen rich)
2000–2030[24,25]	Si–H	stretching (single)
2085–2100[21,24,25]	Si–H	stretching in SiH_2or $(SiH_2)_n$ or on void surfaces
2140–2160[21,24,25]	Si–H	stretching in H_2–Si(SiO) or stretching in SiH_3
2190–2200[3,21,25]	Si–H	stretching in H–Si(O_2Si)
2250–2260[3,21,25]	Si–H	stretching H–Si(O_3)

4.2.1. Si–O–Si related modes

The absorption coefficient spectrum of the sample without oxygen ($R_c = 0$) contains only three components at 460 cm^{-1}, 640 cm^{-1}, and 880 cm^{-1}, as shown in Fig. 5(a). They correspond to the Si–Si stretching mode, the Si–H bending (rocking) mode, and the Si–H scissor mode in SiH_2, respectively. When the oxygen is incorporated into the film, the O-related components at 500 cm^{-1} (Si–O–Si rocking), 790 cm^{-1} (Si–O–Si bending), and 940–1150 cm^{-1} (Si–O–Si stretching) appear and the absorption intensities increase with increasing R_c. Because the measured IR spectra show a high level of noise below 500 cm^{-1}, only the 790 cm^{-1} mode and the 940–1150 cm^{-1} mode will be further discussed here.

Figure 8(a) shows the very good linear relationship of the integrated absorption between the 940–1150 cm^{-1} mode and the 790 cm^{-1} mode. This confirms that these two absorption modes arise from the same group of atoms. The oxygen concentration of the sample is estimated by integrating the absorption of the 940–1150 cm^{-1} mode with the oscillator strength of 0.156 at.%/eV[3] and is shown in Fig. 8(b) as a function of the gas ratio of CO_2 to SiH_4. The increase of R_c effectively enhances the oxygen concentration in the film.

Furthermore, the 940–1150 cm^{-1} mode is deconvoluted into two components at 1050 cm^{-1} and 1135 cm^{-1}. The 1050 cm^{-1} mode is regarded as the Si–O–Si stretching mode when the Si atom is bonded to a single oxygen atom and 1135 cm^{-1} when bonded to more than one oxygen atom (oxygen-rich).[21] The dependence of the relative contribu-

tions of the 1050 cm^{-1} mode and the 1135 cm^{-1} mode on R_c are shown in Fig. 8(c). It can be found that with increasing R_c, although the total amount of oxygen keeps increasing, the relative contribution of the 1050 cm^{-1} mode decreases, while that of the 1135 cm^{-1} mode increases. This suggests that, with increasing oxygen concentration, it is more likely for multiple O atoms to bond with a single Si atom, rather than O atoms primarily bonding one-on-one with Si atoms dispersively. This is consistent with the two-phase structure model[12,28,29] of the a-SiO$_x$:H materials deposited by PECVD using CO_2 as the oxygen source: the film is composed of a silicon-rich phase and an oxygen-rich phase.

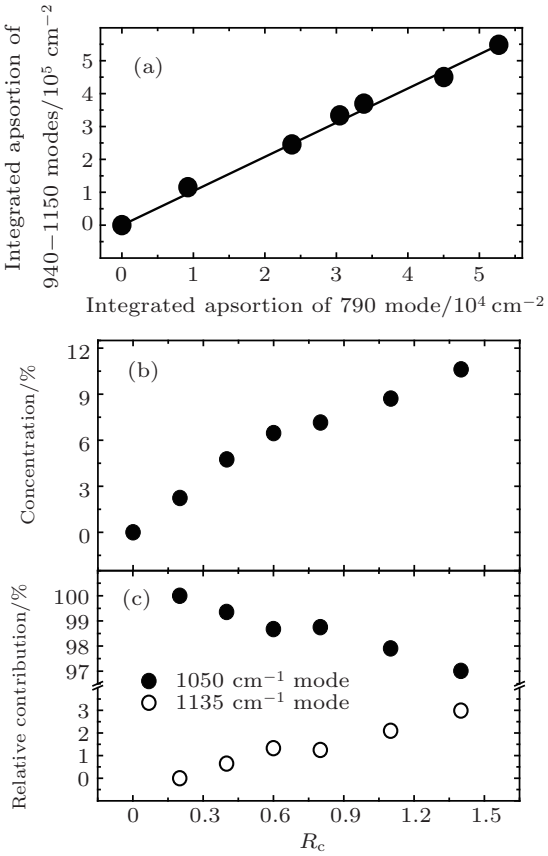


Fig. 8. (a) Relation between the integrated absorption of the 940–1150 cm^{-1} mode and that of the 790 cm^{-1} mode. (b) The dependence of the estimated oxygen concentration on R_c. (c) The dependence of relative contributions of 1050 cm^{-1} and 1135 cm^{-1} modes on R_c.

4.2.2. Si–H related modes

The variation of Si–H related modes will be discussed in this section. As shown in Fig. 5(a), the absorption intensity of the 640 cm^{-1} mode (Si–H bending or rocking in all kinds of Si–H groups) varies only a little throughout the investigated range of R_c. This indicates that, in our case, the hydrogen concentration is not affected much by the amount of O atoms incorporated.

The R_c dependence of absorption for the 2000 cm^{-1}, 2100 cm^{-1}, 2140 cm^{-1}, 2190 cm^{-1}, and 2250 cm^{-1} modes is shown in Fig. 9(a). The modes at 2140 cm^{-1}, 2190 cm^{-1}, and 2250 cm^{-1} arise from Si–H stretching in the O-related groups of H_2–Si(SiO), H–Si(O_2Si), and H–Si(O_3), respectively. They are absent in the a-Si:H layer (R_c =0) but appear and increase as increasing oxygen is incorporated (see Fig. 5(b)). On the other hand, the O incorporation also affects the configuration of Si–H in the groups without oxygen. The 2000 cm^{-1} mode (single Si–H stretching) decreases while the 2100 cm^{-1} mode (Si–H stretching in SiH_2, $(SiH_2)_n$, or voids) increases rapidly with increasing R_c till R_c reaches 0.6, and then both of them stay unchanged when R_c is further increased. It is believed that the 2100 cm^{-1} mode corresponds to the stretching of Si–H or SiH_2 at the surface of nano-scale voids, where it is likely related to the defects in a-Si:H.[30] So it suggests that the defect densities increase with increasing O incorporation at first, and become saturated when the oxygen concentration is higher than a critical point (about 6% in our case). This trend is consistent with the dependence of defect densities in a-SiO$_x$:H films on the oxygen concentration investigated by Bacioglu *et al.*[31] with the constant current method (CPM).

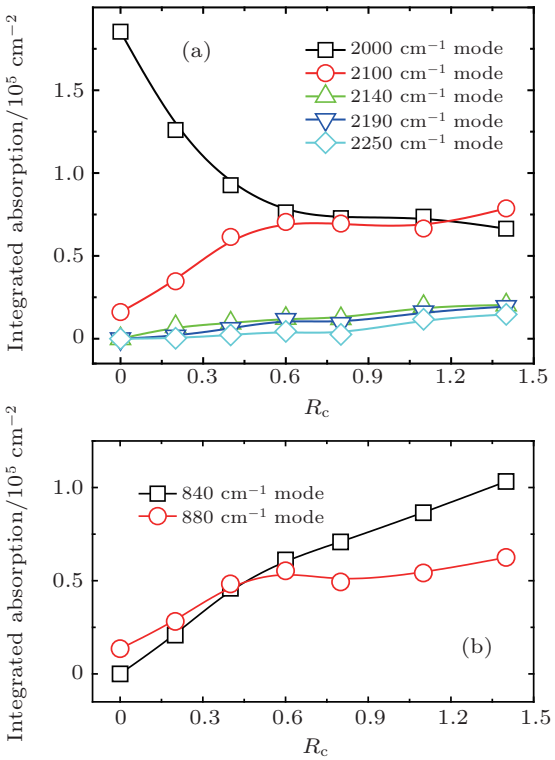


Fig. 9. (color online) (a) Dependence of the integrated absorption of the 2000 cm^{-1}, 2100 cm^{-1}, 2140 cm^{-1}, 2190 cm^{-1}, and 2250 cm^{-1} modes on R_c. (b) Dependence of the integrated absorption of the 840 cm^{-1} and 880 cm^{-1} modes on R_c.

The variation of the integrated absorption 840 cm^{-1} mode with increasing R_c is shown in Fig. 9(b). No 840 cm^{-1} mode is found in the a-Si:H sample, but it increases with increasing R_c throughout the investigated range. As listed in Table 1, the 840 cm^{-1} mode is argued to represent either the Si–H

wagging in $(SiH_2)_n$, the Si–H bending in H–Si(O_2Si), or both. The possible Si–H stretching of $(SiH_2)_n$ and H–Si(O_2Si) can be located at 2100 cm^{-1} and 2190 cm^{-1}, respectively. Consequently, the integrated absorption of these two possible modes and their summation are plotted versus the absorption of the 840 cm^{-1} mode in Fig. 10(a). A good linear relation is found only between the 2190 cm^{-1} mode and the 840 cm^{-1} mode. Combined with the absence of the 840 cm^{-1} mode in the a-Si:H ($R_c = 0$) sample, we suggest that the 840 cm^{-1} mode is only from the Si–H bending in H–Si(O_2Si) and no $(SiH_2)_n$ group exists in our samples.

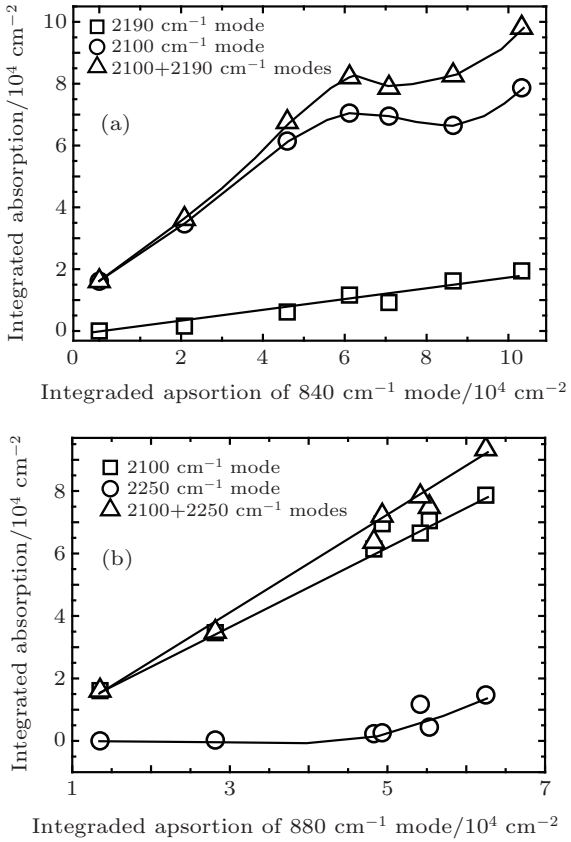


Fig. 10. (a) Relation between the integrated absorption of the 840 cm^{-1} mode and that of the 2100 cm^{-1} mode, 2190 cm^{-1}mode and their summation. (b) Relation between the integrated absorption of the 880 cm^{-1} mode and that of the 2100 cm^{-1} mode, 2250 cm^{-1}mode and their summation.

As also shown in Fig. 9(b), the 880 cm^{-1} mode increases with increasing R_c till 0.6, and then becomes saturated. It also corresponds to two possible components: Si–H scissor in SiH_2 and bending in H–Si(O_3). The stretching modes of these two possible groups are located at 2100 cm^{-1} and 2250 cm^{-1}, respectively. As shown in Fig. 10(b), the 880 cm^{-1} mode linearly relates to both the 2100 cm^{-1} mode and the summation of 2100 cm^{-1} and 2250 cm^{-1} modes. Since the stretching and bending of Si–H in H–Si(O_3) should be reflected at 880 cm^{-1} and 2250 cm^{-1} mutually, we suspect both SiH_2 and H–Si(O_3) contribute to the 880 cm^{-1} mode in our case.

5. Conclusions

By reviewing the different methods used to analyze the IR transmittance of thin film silicon alloys, an improved method based on the Maley model has been proposed to convert the transmittance to the absorption coefficient. It can be implemented easily and will not introduce any extra errors in the process. In particular, with no necessity of empirical correction factors, it is effective for the films with thin thicknesses and other silicon-based alloys with different reflective indexes.

By means of this method, the structural properties of a-SiO_x:H materials that depend on the oxygen concentration have been studied in detail. With increasing oxygen concentration, it becomes more likely that multiple O atoms will bond with a single Si atom. The intensity of the void-related mode at 2100 cm^{-1} increases with increasing O incorporation at first, and becomes saturated when the oxygen concentration is higher than a critical point. The origin of the 840 cm^{-1} and 880 cm^{-1} modes has also been discussed. Based on our results, we conclude that the 840 cm^{-1} mode originates only from the Si–H bending in the H–Si(O_2Si) group and that the Si–H absorption by both SiH_2 and H–Si(O_3) is responsible for the 880 cm^{-1} mode.

Acknowledgments

The authors gratefully acknowledge Dr. He Zhang for the helpful discussion, Dr. Tao Chen for the revision of manuscript, and Qi Tang for the help in program compilation.

References

[1] Sriprapha K, Piromjit C, Limmanee A and Sritharathikhun J 2011 *Sol. Energ. Mat. Sol. C.* **95** 115
[2] Inthisang S, Krajangsang T, Yunaz I A, Yamada A, Konagai M and Wronski C R 2011 *Phys. Status Solidi C* **8** 2990
[3] Lucovsky G, Yang J, Chao S S, Tyler J E and Czubatyj W 1983 *Phys. Rev. B* **28** 3223
[4] Lucovsky G and Pollard W 1984 *T Topics in Applied Physics* (Berlin: Springer) p. 301
[5] Smets A H M, Matsui T, Kondo M and van de Sanden M C M 2009 *34th IEEE Photovoltaic Specialists Conference*, 7–12 June 2009 New York, US, p. 721
[6] Brodsky M H, Cardona M and Cuomo J J 1977 *Phys. Rev. B* **16** 3556
[7] Connell G A N and Lewis A 1973 *Phys. Status Solidi B* **60** 291
[8] He L N, Wang D M and Hasegawa S 2000 *J. Non-Cryst. Solids* **261** 67
[9] Mukhopadhyay S and Ray S 2011 *Appl. Surf. Sci.* **257** 9717
[10] Matsumoto Y, Yu Z R and Sanchez R V 2008 *Sol. Energ. Mat. Sol. C* **92** 576
[11] Riera M, Rodríguez J A, Barreto J and Domínguez C 2007 *Thin Solid Films* **515** 3380
[12] Haga K and Watanabe H 1996 *J. Non-Cryst. Solids* **195** 72
[13] He L, Inokuma T, Kurata Y and Hasegawa S 1995 *J. Non-Cryst. Solids* **185** 249
[14] Maley N 1992 *Phys. Rev. B* **46** 2078
[15] Langford A A, Fleet M L, Nelson B P, Lanford W A and Maley N 1992 *Phys. Rev. B* **45** 13367
[16] Manfredotti C, Fizzotti F, Boero M, Pastorino P, Polesello P and Vittone E 1994 *Phys. Rev. B* **50** 18046

[17] Lambertz A, Grundler T and Finger F 2011 *J. Appl. Phys.* **109** 113109
[18] Zhang X D, Yue Q, Zheng X X, Geng X H and Zhao Y 2011 *Thin Solid Films* **520** 684
[19] Veneri P D, Mercaldo L V and Usatii I 2010 *Appl. Phys. Lett.* **97** 23512
[20] Arup S and Debajyoti D 2009 *J. Phys. D: Appl. Phys.* **42** 215404
[21] Babal P, Blanker J, Vasudevan R, Smets A H M and Zeman M 2012 *38th IEEE Photovoltaic Specialists Conference (PVSC),* 3–8 June 2012 Austin, US, p. 321
[22] Shen S C, Fang C J, Cardona M and Genzel L 1980 *Phys. Rev. B* **22** 2913
[23] Lucovsky G, Yang J, Chao S S, Tyler J E and Czubatyj W 1984 *Phys. Rev. B* **29** 2302
[24] Lucovsky G, Nemanich R J and Knights J C 1979 *Phys. Rev. B* **19** 2064
[25] Samanta A and Das D 2009 *Sol. Energ. Mat. Sol. C.* **93** 588
[26] Das D, Jana M and Barua A K 2000 *Sol. Energ. Mat. Sol. C.* **63** 285
[27] Pai P G, Chao S S, Takagi Y and Lucovsky G 1986 *Journal of Vacuum Science & Technology A: Vacuum, Surfaces, and Films* **4** 689
[28] Wang Y Q, Chen C Y, Chen W D, Yang F H and Diao H W 2001 *Acta Phys. Sin.* **50** 2418 (in Chinese)
[29] Watanabe H, Haga K and Lohner T 1993 *J. Non-Cryst. Solids* **164–166** 1085
[30] Smets A H M, Kessels W M M and van de Sanden M C M 2003 *Appl. Phys. Lett.* **82** 1547
[31] Bacioglu A, Kodolbas A O and Oktu O 2005 *Sol. Energ. Mat. Sol. C* **89** 49